

5-11-2016

# Tau and A $\beta$ imaging, CSF measures, and cognition in Alzheimer's disease

Matthew R. Brier

Brian Gordon

Karl Friedrichsen

John E. McCarthy


Washington University in St Louis, mccarthy@wustl.edu

Ari Stern

Washington University in Saint Louis, stern@wustl.edu

*See next page for additional authors*

Follow this and additional works at: [https://openscholarship.wustl.edu/math\\_facpubs](https://openscholarship.wustl.edu/math_facpubs)

 Part of the [Applied Mathematics Commons](#), [Cognitive Neuroscience Commons](#), [Neurology Commons](#), and the [Other Analytical, Diagnostic and Therapeutic Techniques and Equipment Commons](#)

---

## Recommended Citation

Brier, Matthew R.; Gordon, Brian; Friedrichsen, Karl; McCarthy, John E.; Stern, Ari; Christensen, Jon; Owen, Christopher; Aldea, Patricia; Su, Yi; Hassenstab, Jason; Cairns, Nigel J.; Holtzman, David M.; Fagan, Anne M.; Morris, John C.; Benzinger, Tammie L.S.; and Ances, Beau M., "Tau and A $\beta$  imaging, CSF measures, and cognition in Alzheimer's disease" (2016). *Mathematics Faculty Publications*. 34.

[https://openscholarship.wustl.edu/math\\_facpubs/34](https://openscholarship.wustl.edu/math_facpubs/34)

This Article is brought to you for free and open access by the Mathematics and Statistics at Washington University Open Scholarship. It has been accepted for inclusion in Mathematics Faculty Publications by an authorized administrator of Washington University Open Scholarship. For more information, please contact [digital@wumail.wustl.edu](mailto:digital@wumail.wustl.edu).

---

**Authors**

Matthew R. Brier, Brian Gordon, Karl Friedrichsen, John E. McCarthy, Ari Stern, Jon Christensen, Christopher Owen, Patricia Aldea, Yi Su, Jason Hassenstab, Nigel J. Cairns, David M. Holtzman, Anne M. Fagan, John C. Morris, Tammie L.S. Benzinger, and Beau M. Ances

**Title:** Tau Imaging Relationships with Amyloid  $\beta$  Imaging, CSF tau/A $\beta_{42}$ , and Cognition in Alzheimer's Disease

**Authors:** Matthew R. Brier<sup>1</sup>, Brian Gordon<sup>2,3</sup>, Karl Friedrichsen<sup>2</sup>, John McCarthy<sup>4</sup>, Ari Stern<sup>4</sup>, Jon Christensen<sup>2</sup>, Christopher Owen<sup>2</sup>, Patricia Aldea<sup>2</sup>, Yi Su<sup>2</sup>, Jason Hassenstab<sup>1,3</sup>, Nigel J. Cairns<sup>1,3,5</sup>, David M. Holtzman<sup>1,3,7</sup>, Anne M. Fagan<sup>1,3,7</sup>, John C. Morris<sup>1,3,5,7</sup>, Beau M. Ances<sup>1,2,3,7\*</sup>, Tammie L.S. Benzinger<sup>2,3,6\*</sup>

\*Contributed equally

**Affiliations:** Departments of <sup>1</sup>Neurology, <sup>2</sup>Radiology, <sup>3</sup>Knight Alzheimer's Disease Research Center, <sup>4</sup>Mathematics, <sup>5</sup>Pathology, <sup>6</sup>Neurosurgery, and the <sup>7</sup>Hope Center for Neurological Disorders, Washington University in St Louis.

**One sentence summary:** Pathological tau PET imaging more closely correlates with Alzheimer's disease-related cognitive impairment than amyloid-beta imaging; distinct patterns of tau deposition are identified.

**Correspondence To:**

Beau Ances, MD PhD  
Department of Neurology  
Washington University in St Louis  
bances@wustl.edu

## **Abstract**

Alzheimer's disease (AD) is characterized by two molecular pathologies: cerebral beta-amyloidosis (amyloid-beta [ $A\beta$ ] plaques) and tauopathy (neurofibrillary tangles, neuritic plaques and neuropil threads). Until recently, only  $A\beta$  topographies could be studied *in vivo* in humans owing to a lack of tau positron emission tomography (PET) imaging agents. Current clinic-pathological studies link tau pathology closely to the onset and progression of cognitive symptoms AD. This study reports on PET tau and  $A\beta$  imaging results in a cohort of cognitively normal older adults and those with very mild AD. Multivariate analyses identified unique disease-related spatial topographies in both tau and  $A\beta$  deposition. These PET tau and  $A\beta$  topographies were spatially unique but strongly related. Cerebrospinal fluid measures of tau, often used to stage preclinical AD, were strongly correlated with tau deposition in the temporal lobe. Tau deposition in the temporal lobe more closely tracked dementia status and was a better predictor of cognitive performance than  $A\beta$  deposition in any region of the brain. These data support models of AD where tau pathology closely tracks changes in brain function responsible for the onset of early symptoms.

## **Introduction**

Alzheimer's disease (AD) is characterized neuropathologically by the presence of amyloid-beta ( $A\beta$ ) plaques and tau-immunoreactive neuritic plaques, neurofibrillary tangles and neuropil threads in the cerebral cortex (1). Autopsy studies demonstrate that  $A\beta$  and tau pathology accumulate in stereotypical spatial

patterns, or topographies, over the course of the disease (2, 3). Topographic studies of AD-related pathology *in vivo*, until recently, have been limited to fibrillar A $\beta$  (4, 5) owing to a lack of positron emission tomography (PET) tau pathology imaging agents. However, a number of tau pathology imaging agents have recently been developed and are available for human studies (6).

Extant models of AD pathophysiology establish a temporal ordering of biomarkers, with the emergence of AD-related tauopathy occurring downstream to the accrual of A $\beta$  pathology (7-11). Consistent with this proposal, markers of tau pathology correlate more closely with changes in cognition compared to A $\beta$  measures (12). However, the prior lack of imaging agents has limited studies of tau to post-mortem examinations (13-16) or measures that lack topographic information (i.e., cerebrospinal fluid [CSF]). As a result, relationships between cognition and A $\beta$  topography have been defined (17), but the relationship with tau topography is not defined *in vivo*. Without this spatial information, CSF tau measures may be assessing other forms of neurodegeneration related to cell death or synaptic dysfunction.

The use of both tau and A $\beta$  imaging allows for the attribution of AD-related cognitive dysfunction to specific pathological process and locations within the brain. Further, the spatial relationships between tau pathology and other biomarkers of AD are not established. This report examines how tau imaging topographies relate to clinical status, A $\beta$  imaging, CSF measures of AD pathology, and

neuropsychological performance. Tau and A $\beta$  represent distinct pathological processes but they are strongly related in the context of AD. Given that PET- and CSF-based techniques may measure similar processes (18), PET and CSF measurements of tau and A $\beta$  are hypothesized to be related but that relationship is likely stronger within specific topographies. Next, the relationship between tau and A $\beta$  imaging with cognition was assessed. Given extant models (8, 9) and limited autopsy-based empirical data (13-15) it was hypothesized that tau would be a stronger predictor of cognition than A $\beta$  owing to its place later in preclinical disease course. These relationships are investigated *in vivo* for the first time using multivariate statistical models well suited to identify PET topographies associated with presence or absence of disease, identify relationships between A $\beta$  and tau pathology in distinct topographies, and describe the relationship with CSF and neuropsychological measures of disease.

## **Results**

Data from forty-six individuals was examined. Global cognitive and functional performance was assessed by the clinical dementia rating (CDR) (19). Each participant underwent T807 (tau) (20) and florbetapir (A $\beta$ ) positron emission tomography (PET) and magnetic resonance imaging (MRI). A subset also underwent lumbar puncture for CSF assays and/or neuropsychological testing. Demographics of each subset of the cohort are provided in Table 1. Standardized uptake value ratios (SUVR) with (when presenting regional data) and without (when presenting voxelwise data) partial volume correction were calculated within 42 bilateral

anatomical regions of interest (ROI) defined by FreeSurfer (21, 22). For additional methodological detail throughout, see Methods and Supplemental Material.

### Clinically Impaired Participants Demonstrate Elevated Tau Burden

Mean (across participants) tau and A $\beta$  SUVR images are shown in Figure 1; representative single subject data are shown in Supplemental Figure 1. The data were split into two groups based on the presence or absence of cognitive impairment. Cognitively normal (CDR 0;  $N = 36$ ) participants show minimal tau tracer uptake throughout the brain with the exception of the basal ganglia. Cognitively impaired (CDR > 0;  $N = 10$ ) participants exhibited markedly increased uptake in the temporal lobes and throughout the cortex. The A $\beta$  images demonstrate the known separation between cognitively normal and cognitively impaired groups.

### Distinct Tau and A $\beta$ Topographies are Associated with Cognitive Impairment

To assess the behavior of PET tau and A $\beta$  pathology across participants, the imaging data were first decomposed into component topographies. This accomplishes two goals: 1) accounts for the correlation structure of the data across ROIs and 2) reduces the number of statistical comparisons. Thus, singular value decomposition (SVD) identifies a small number of latent component topographies whose representation in single subjects explains a majority of the variance. In each participant, PET tau and A $\beta$  pathology burden was assessed in 42 ROIs, however, many ROIs are highly correlated and can be more concisely summarized as topographies, or combinations, of ROIs. The PET tau and A $\beta$  data were arranged into

participant (N=46) by ROI (M=42) matrices separately and subjected to SVD. PET tau and A $\beta$  each were best described as a combination of two component topographies (Figure 2A). Both PET tau and A $\beta$  demonstrated empirically determined rank 2 suggesting that the two biomarkers have similar signal to noise characteristics. For both PET tau and A $\beta$ , the first topography roughly corresponded to the mean of the image (i.e., regions are similarly positively weighted). The second PET tau topography was most strongly loaded in the temporal lobe including the hippocampus. In contrast, the second PET A $\beta$  topography was most strongly loaded in frontal and parietal regions. This analysis demonstrates that both PET tau and A $\beta$  data exhibit strong autocorrelation across ROIs but each has distinct topographies.

In each participant, the representation of each of the 2 PET tau and 2 PET A $\beta$  topographies described above was best estimated using regional weights derived from the SVD. For each topography, these values were subjected to an ANCOVA with age, CDR, and presence of an apolipoprotein (APOE )  $\epsilon$ 4 allele as factors (Supplemental Table 1). The two PET tau topographies were more strongly represented in participants with higher CDR status ( $p < 0.001$ ) but were not significantly modified by age or APOE status (Figure 2B). The first PET A $\beta$  topography was not significantly associated with any variables of interest, however the second topography was more strongly represented in participants with higher CDR status ( $p = 0.04$ ) and moderately associated with increasing age ( $p = 0.08$ ). In both the tau and A $\beta$  data there are statistically significant differences between the CDR 0 and CDR>0 groups, however there is significant overlap particularly in the A $\beta$



result. The separation between the CDR 0 and CDR>0 groups was more marked in the PET tau data compared to the PET A $\beta$  data. This visual observation is quantified as *F* values that are an order of magnitude larger for PET tau compared to PET A $\beta$  (Supplemental Table 1). Thus, as measured by the CDR, representation of tau topographies more strongly associates with dementia status across participants.

### Evidence of Preclinical AD is Associated with Pathological Topographies

Inspection of Figure 2B reveals that expression of the each topography varies widely in the CDR 0 participants, particularly with respect to PET A $\beta$  topographies. CDR 0 implies cognitive normality but not absence of preclinical pathology. Preclinical AD can be operationalized using CSF measures of tau and A $\beta$  with simple scalar cutoffs. To most simply characterize the pathological status of the CDR 0 participants, median splits were used to dichotomize participants as either CSF A $\beta$  $\pm$  or tau $\pm$ . A $\beta$  $^-$ , tau $^-$  corresponds to healthy aging without pathology; A $\beta$  $^+$ , tau $^-$  corresponds to Stage 1 preclinical disease; A $\beta$  $^+$ , tau $^+$  corresponds to Stage 2 preclinical disease (23, 24). Stratifying CDR 0 participants in this manner reveals that CDR 0 participants with higher expression of the component topographies tend to have CSF evidence of elevated A $\beta$  or tau pathology (Figure 2C). The effect of preclinical disease stage is more marked on PET A $\beta$ , suggesting that tau pathology burden is more closely temporally linked to clinical status as measured by CDR and preclinical disease stage. The preceding results were reproduced in a larger sample who only had PET tau data available (See Supplemental Results).

### PET Tau and A $\beta$ , in Distinct Topographies, are Strongly Correlated

The previous analysis described the relationship between PET tau and A $\beta$  topographies and disease stage. Next, the relationship between the PET tau and A $\beta$  topographies was compared directly using canonical correlation. Canonical correlation is a multivariate generalization of the more familiar bivariate correlation. Canonical correlation identifies both a PET tau and PET A $\beta$  topography such that the data, when projected onto these weighted topographies, are maximally correlated. Thus, canonical correlation identifies the topography of each pathological species that is most related to the other species. The present PET tau and A $\beta$  topographies were represented by a single canonical correlation that explained 75% of the covariance in the data (Figure 3). The weighted regional patterns of the two topographies were modestly correlated ( $r = 0.29$ ,  $p = 0.062$ ), which reflects the known divergence in the pathologic topographies (2, 3). The PET data weighted and averaged according to these topographies were highly correlated ( $r = 0.92$ ,  $p < 10^{-18}$ ), which reflects the strong relationship between tau and A $\beta$  when the appropriate topographies are considered. The PET tau topography that was most heavily loaded in medial temporal lobe, parietal cortex, and precuneus and was most highly correlated with PET A $\beta$  topography in the frontal and parietal regions.

### Mean PET tau and A $\beta$ are Correlated with CSF tau, p-tau, and A $\beta_{42}$

PET tau and A $\beta$  imaging techniques and CSF based techniques may measure correlated pathological processes (18). Therefore, the two measures may be related.

To investigate this relationship, the correlations between mean (calculated across all grey matter regions) PET tau and A $\beta$  and CSF tau, phosphorylated tau (p-tau), and A $\beta_{42}$  were calculated (Supplemental Table 2). As predicted, mean PET tau was positively correlated with CSF tau ( $r = 0.36$ ,  $p = 0.029$ ) and CSF p-tau ( $r = 0.29$ ,  $p = 0.089$ ) but was not significantly correlated with CSF A $\beta_{42}$  ( $r = -0.25$ ,  $p = 0.14$ ); mean PET A $\beta$  was negatively correlated with CSF A $\beta_{42}$  ( $r = -0.54$ ,  $p = 0.006$ ) but also positively correlated with CSF tau ( $r = 0.52$ ,  $p = 0.0011$ ) and p-tau ( $r = 0.49$ ,  $p = 0.0023$ ). The negative correlations owe to CSF A $\beta_{42}$  being reduced, not increased, by the AD process as more A $\beta$  becomes deposited in the brain. Therefore, the PET and CSF techniques are strongly correlated measures of AD pathological processes. However, the strengths of these relationships were not remarkably strong and vary across biomarkers. The limited strength of these correlations may owe to the PET ~ CSF relationship only being strong within particular topographies; that topographic information is necessarily averaged across in this analysis.

#### CSF Tau and A $\beta_{42}$ are Correlated with Specific Topographies of PET tau and A $\beta$

Penalized regression models (25-27) with either CSF tau or A $\beta_{42}$  (separately) as an outcome and regional PET tau and A $\beta$  SUVR (together) as predictors were fit to determine the relationship between CSF and regional PET measures. PET tau and A $\beta$  topographies were considered together in the model allowing for the data to determine the modality that best predicted the variable of interest. The critical feature of penalized regression is that the solution is sparse (i.e., the regression  $\beta$ s corresponding to most PET tau and A $\beta$  ROIs are set to zero) and only the most

predictive ROIs receive non-zero regression  $\beta$  weights. The relationship between PET tau and A $\beta$  topographies and CSF tau was examined first. The penalized model significantly fit the data ( $R^2 = 0.96$ ;  $Z = 4.72$ ;  $p < 0.0001$ ). The combination of PET tau and A $\beta$  topographies that best correlate with CSF tau are shown in the top row of Figure 4A (Exact values shown in Supplemental Table 3). CSF tau was equally related to PET tau ( $\sum|\beta_{\tau_{\text{tau}}}| = 2.93$ ) and PET A $\beta$  ( $\sum|\beta_{A\beta}| = 2.54$ ), as measured by the sum of the absolute value of the regression  $\beta$  values corresponding to PET tau and A $\beta$  ROIs, respectively. This equal weighting is consistent with tau pathology being dependent on initial A $\beta$  accumulation. Predictive PET tau regions include entorhinal and temporal cortex and the cuneus. The PET A $\beta$  contribution was derived from temporal and frontal regions. Similar topographies of predictive PET regions of interest were found when predicting CSF p-tau; the overall correlation between the CSF tau and CSF p-tau predictive topographies was high ( $r = 0.77$ ,  $p < 10^{-16}$ ).

Next, the same relationship was investigated but with CSF A $\beta_{42}$  as the predicted outcome variable. The penalized model significantly fit the data ( $R^2 = 0.34$ ;  $Z = 3.22$ ;  $p = 0.0006$ ). The joint topographies of PET tau and A $\beta$  that best correlates with CSF A $\beta_{42}$  are shown in the bottom row of Figure 4A (Exact values shown in Supplemental Table 3). Most of the regression  $\beta$  values are negative owing to the inverse relationship between CSF A $\beta$  and pathology burden. In contrast to the CSF tau model, the predictive weight is more skewed towards PET A $\beta$  ( $\sum|\beta_{A\beta}| = 0.46$ ) compared to PET tau ( $\sum|\beta_{\tau_{\text{tau}}}| = 0.26$ ). This suggests that PET tau has

relatively less predictive information relating to CSF A $\beta$ <sub>42</sub>. The contributing topography from PET tau was primarily loaded in the superior portions of the cortex. The PET A $\beta$  topography is composed primarily of frontal and parietal regions. The highly significant predictive power of both models suggests that there is a strong relationship between CSF and PET measures of tau and A $\beta$  pathology.

### Specific tau and A $\beta$ Topographies Correlate with Neuropsychological Performance

To examine the relationship between pathology and cognitive function, the relationship between PET tau and A $\beta$  topographies and neuropsychological composite scores was compared using the same penalized regression model as described above. Each participant underwent neuropsychological testing that is summarized into four composite scores summarizing the domains of episodic, semantic, working memory, and visuospatial processing and an additional overall (global) measure. Of these, episodic ( $Z = 2.42$ ;  $p = 0.0078$ ), semantic ( $Z = 4.85$ ;  $p < 0.0001$ ), visuospatial ( $Z = 5.17$ ;  $p < 0.0001$ ) and the global score ( $Z = 3.97$ ;  $p < 0.0001$ ) were significantly predicted by penalized regression after correction for multiple comparisons while the working memory composite was not significantly fit by the model. The combined PET tau and A $\beta$  topographies that best predict each cognitive composite are shown in Figure 4B (Exact values shown in Supplemental Table 3). In each case, PET tau was the dominant topography with contributions to the model, quantified as the sum of the absolute value of the regression  $\beta$ , two- to nine-fold higher than the contribution of PET A $\beta$ . With the exception of predicting episodic memory, the topographies were sparse, including only temporal regions

and basal frontal regions. The overwhelming contribution of PET tau, specifically temporal lobe tau, in each tested domain demonstrates that tau is more closely related to cognition compared to A $\beta$ .

We further investigated the correlation between PET tau and A $\beta$  topography and neuropsychological composite scores in the CDR 0 group only. In the domains that were significantly associated with PET tau and A $\beta$  topographies in the full group, we refit the models in the CDR 0 group only and calculated the correlation between the resulting predictive topographies. The topography that was predictive of episodic memory scores in the full group was not correlated with predictive topography in the CDR 0 group ( $r = 0.04$ ,  $p = 0.70$ ). Similarly, the topographies predictive of semantic memory performance were not significantly correlated ( $r = -0.01$ ,  $r = 0.90$ ). However, the topographies predicting visuospatial performance ( $r = 0.54$ ,  $p < 0.001$ ) and global cognitive performance ( $r = 0.19$ ,  $r = 0.091$ ) were correlated, albeit the latter at a trend level. These data suggest that the relationship between pathology and neuropsychological performance varies over the course of the disease.

## **Discussion**

The present results identified topographies of tau deposition as measured by T807 PET that were associated with clinical status, PET A $\beta$  deposition, CSF AD biomarkers, and AD-related cognitive impairment. A strong correlation existed between A $\beta$  deposited in one topography and tau deposited in another topography. Tau imaging, both globally and in a specific topography, was significantly associated

with CSF measures of tau-related neural injury. In a combined model, PET tau deposition was demonstrated to be more closely associated with cognitive function than A $\beta$  imaging. Together, these results establish tau imaging as a robust and important biomarker of AD-related pathology.

The A $\beta$  imaging literature is vast and has developed over more than a decade (4), however tau imaging is a relatively new addition to the field. FDDNP was the first tau imaging agent but had low signal to noise properties and also binds to A $\beta$ , which precluded investigation of specific pathological species (28) or required co-imaging with A $\beta$  agents and elaborate subtraction procedures (29). Methodological studies (i.e., biochemistry and small animal studies) have identified several compounds that are specific to tau pathology and possess favorable biochemical properties (30, 31). Human studies have, to date, have been small (N<25) and identified PET tau topographies consistent with post-mortem studies (20, 32-35). In this preliminary body of work, PET tau pathology burden in specific regions of interest (e.g., hippocampus) were more strongly correlated with cognitive performance and hippocampal volume (34, 35). These studies have demonstrated the utility of tau imaging agents in identifying tau pathology burden *in vivo*. The present study builds on those studies by examining a larger cohort at various disease stages and capitalizing upon the spatial information of PET by explicitly relating tau topographies to disease stage, A $\beta$  imaging, CSF biomarker, and cognition.

PET tau and A $\beta$  imaging acquires data at the resolution of approximately 5 to 8mm and sampled as many thousands of voxels, but the true dimensionality of the data is likely much lower (36). This study identified two topographies for both PET tau and A $\beta$  that explained most of the variance in the data. The two tau topographies were associated with disease severity as measured by the CDR. The first tau topography was homogeneously distributed across the brain but the second was concentrated in the temporal lobe. Similarly the first A $\beta$  topography was broadly distributed across the brain, while the second A $\beta$  topography loaded more focally in frontal and parietal regions and was significantly associated with disease stage. Notably, the separation between CDR groups was visually more marked with respect to tau burden (Figure 2B and C), though significant overlap remains. Overlap with respect to CDR status likely represents the variable relationship between pathological burden and cognitive symptoms often attributed to differences in host factors, e.g., cognitive reserve (8, 23). This suggests that representation of pathologically associated topographies of both tau and A $\beta$  index disease progression but the relationship to cognitive impairment is more pronounced with respect to tau.

A unique feature of AD is that it is a dual proteinopathy. Indeed one of the more debated mechanisms is how two pathological species progress in independent topographies (11, 37, 38). While the topographies are distinct, this study uses canonical correlation to emphasize that these two processes are related. In fact, the correlation between tau and A $\beta$  can be remarkably high when the relevant



topographies are considered. This suggests that, for a given severity of A $\beta$  deposition, the severity of tau pathology can also be estimated. The mechanism underlying the relationship between A $\beta$  and tau in the generation of AD is unclear, but the empirical relationship is clearly evident.

In the absence of widely used tau PET ligands, CSF-based measurements of tau pathology burden have predominated the AD field (39). CSF-based measurements afford certain advantages (e.g., broad applicability) but do not provide topographic information afforded by PET. Nevertheless, CSF-based measures and PET-based measures index similar pathological processes in the context of AD. As a result, a high correlation between mean PET tau SUVR and CSF tau is expected. Perhaps less intuitive, but commonly observed, is the strong relationship between CSF tau and PET A $\beta$  SUVR, even in the absence of neurofibrillary tangles (40). This relationship could be understood in terms of the ordered nature of biomarker progression; once detectable tau pathology is present there is already advanced A $\beta$  pathology, allowing for a significant relationship (8, 9). More importantly, the relationship between CSF and PET derived measures were topographically specific. The specificity of this relationship strengthens the argument that the identified relationships are disease specific: elevated tau in the CSF is associated with tau deposition within regions known to be sensitive to AD-related tauopathy (2). Taken together, these lines of evidence suggest that the desired pathological process is being measured by both techniques.

Understanding the contribution of tau and A $\beta$  to cognitive symptoms, particularly early in AD, has been restricted owing to the lack of topographic tau information *in vivo*. In this study, the predictive power of PET tau and A $\beta$  topographies on neuropsychological performance was evaluated. In each investigated cognitive domain, the weight assigned to PET tau in the best fitting model was larger than the weight assigned to PET A $\beta$ . This implies that tau burden, not A $\beta$  burden, is more closely linked to cognition. This increased correlation suggests that tau and cognition are more closely linked, consistent with extant models of AD (8, 9). Further, PET imaging data coupled with the present penalized regression approach also provides regional specificity. Temporal lobe tau tended to be the strongest predictor of cognitive performance consistent with known focus of tau pathology. The selective nature of the present models suggests that tauopathy severity in the temporal lobe is sufficient to predict cognitive impairment across the early disease stages investigated here.

Taken together, these data provide important insight into the relationship between tau topographies and other measures of AD pathology and cognitive symptoms. This inference is made possible by the emergence of PET tau imaging agents. Tau imaging accurately discriminates disease stage assessed by the CDR, strongly correlates with CSF measures, in particular within temporal regions, and is more related to cognitive performance than A $\beta$  imaging. Thus, tau pathology appears to be more closely linked to cognitive dysfunction consistent with existing hypotheses. These data suggest distinct roles of PET A $\beta$  and tau imaging going

forward. PET A $\beta$  will likely remain a powerful tool for early detection of AD pathology during the preclinical period. However, these data suggest a close relationship between PET tau and disease stage and symptomatology will be critical for tracking the efficacy of disease modifying therapies.

## **Materials and Methods**

### Study Design

Forty-six participants were recruited from ongoing studies of memory and aging at the Knight Alzheimer Disease Research Center at Washington University in St Louis. Participants underwent cognitive assessment with the clinical dementia rating (CDR) (19), MRI and PET imaging with T807 and Florbetapir. All participants with CDR>0 (i.e., clinically impaired) carried clinical diagnoses of Alzheimer's disease or mild cognitive impairment due to Alzheimer's disease. A subset of participants also underwent lumbar puncture (N=36) and neuropsychological assessment (N=40). All participants or their designees provided written informed consent prior to participating in this study that was consistent with the regulations of the Washington University in St Louis School of Medicine Institutional Review Board.

### Neuropsychological Assessment

A comprehensive neuropsychological battery was administered to all participants, typically within two weeks of the annual clinical assessment. Standardized test scores were averaged to form four composites [see

(41) for details on construction of composites and the standardization sample]. The episodic memory composite included the sum of the three free recall trials from the Selective Reminding Test (42), Associate Learning from the Wechsler Memory Scale (WMS) (43), and immediate recall of the WMS Logical Memory or Wechsler Memory Scale-Revised (WMS-R) (44) Logical Memory. The semantic composite included the Information subtest from the Wechsler Adult Intelligence Scale (WAIS) (45), the Boston Naming Test (46), and Animal Naming (46). The working memory composite included WMS Mental Control, Digit Span Forward and Digit Span Backward, and Letter Fluency for S and P. The visuospatial composite included the WAIS Block Design and Digit Symbol subtests and Trailmaking Test A and B (47).

### Imaging

MRI and florbetapir data were acquired on a Biograph mMR scanner (Siemens Medical Solutions, Erlangen, Germany) in a single session. T807 data were acquired in a separate session on a Biograph 40 PET/CT scanner. Participants received a single intravenous (IV) bolus injection of 10 mCi of florbetapir and a single IV bolus injection of 6.5-10 mCi of T807.

PET data were analyzed using our standard technique (18, 19) implemented in the PET unified pipeline (<http://github.com/ysu001/PUP>). FreeSurfer segmentation (44) (<http://freesurfer.net/>) was used as the basis of the quantitative analysis to obtain regional standardized uptake value ratio (SUVR) with cerebellar gray matter as the reference region. Partial volume correction was also performed using a regional spread function (RSF) technique (19). For florbetapir PET, the data

between 50-70 minutes post-injection were used for the analysis; and for T807, the imaging data between 80-100 minutes were used instead.

### CSF Analysis

CSF (20-30 mL) was collected after overnight fasting as described previously (48, 49). Total and phosphorylated tau and A $\beta$ <sub>42</sub> were measured using ELISA (INNOTEST; Fujirebio, formerly Innogenetics, Ghent, Belgium).

### Dimensionality Reduction and Analysis of a Single PET Modality

PET SUVR, for both T807 and Florbetapir, can be measured at the resolution of voxels, structurally or functionally defined sets of voxels, or the entire brain. This gives rise to datasets that appear to be high dimensional (i.e., many samples per imaging session) but can be represented by lower dimensional projections. These bases can be identified using singular value decomposition (SVD) or related procedures (e.g., principal component analysis). In PET data, these composite factors represent topographies (i.e., the weighted combination of brain regions) and the contribution of a given topography to an individual participant's data can be estimated. SVD was performed on the regional SUVR values (as variables) across participants (as samples) for tau and A $\beta$  separately. The number of significant factors was determined by a permutation test.

### Identifying the Relationship Between Tau and A $\beta$ Topographies and CSF and Neuropsychological Performance Using Penalized Regression

Penalized regression was used to identify the relationship between CSF tau and  $A\beta_{42}$  or neuropsychological  $Z$  scores, as outcome variables, and PET tau and  $A\beta$  topographies (as predictors). The penalty in penalized regression is enforced against the estimated regression  $\beta$ s (26). The family of penalized regression fit here is the elastic-net penalty (27): the L1 penalty component enforces sparsity (i.e., many  $\beta$ s will be identically 0, not included in the model) (26) while the L2 penalty allows highly correlated variables to enter the model simultaneously (27). Elastic-net models are well suited for data that are highly collinear such as regional PET data. Model parameters (total penalty and relative contribution of L1 and L2 penalty) are chosen by cross-validation. Penalized regression models, like any machine learning algorithm, are prone to overfitting. To assess significance of the fit models, permutation resampling determined the distribution of  $R^2$  values under the null hypothesis.

#### Canonical Correlation Identifies Relationships Between Tau and $A\beta$ Topographies

Description of the correlation between tau and  $A\beta$  topographies is accomplished using canonical correlation (50, 51). Canonical correlation is the multivariate generalization of the more familiar, e.g., Pearson bivariate correlation. Canonical correlation identifies the weighted average of ROIs in one distribution that is maximally correlated with another weighted average of ROIs in another distribution. The weighting vectors, or canonical vectors, define topographies.

## List of Supplemental Material

1. Supplemental Methods
2. Supplemental Results
3. Supplemental Table 1. ANOVA results related to SVD topographies.
4. Supplemental Table 2. Mean PET and CSF Correlation Matrix.
5. Supplemental Table 3: Regional Regression  $\beta$  Values.
6. Supplemental Table 4: Comparison of BET tau SVD ANOVA results
7. Supplemental Table 5: LOO Analysis results
8. Supplemental Figure 1: PET tau and A $\beta$  SUVR images from single subjects.

**Acknowledgements.** This study was funded by the NIH grants P50AG05681, P01AG003991, P01AG026276, 5P30NS048056, 2UL1TR000448, 5R01AG04343404. Funding was also provided by the Charles F. and Joanne Knight Alzheimer's Research Initiative, Hope Center for Neurological Disorders, and the generous support from Fred Simmons and Olga Mohan and the Paula and Rodger Riney Fund. Avid Radiopharmaceuticals (a wholly owned subsidiary of Eli Lilly) provided florbetapir doses and partial financial support for the florbetapir scanning sessions as well as provided precursor for T807 and radiopharmaceutical chemistry and technology for the Washington University IND under which this was performed. MRB developed methodology, performed formal analysis, and wrote the paper; BG performed formal analysis; KF curated the data and developed methodology; JM and AS developed methodology and computation; JC performed formal analysis and curated the data; PA performed project administration; YI developed methodology; JH contributed resources; NJC, DMH, AMF, JCM contributed to study conception, contributed resources, and project administration; BMA and TLSB provided supervision, conception of the study. All authors critically revised the manuscript.

## References

1. K. Blennow, M. J. de Leon, H. Zetterberg, Alzheimer's disease. *The Lancet* **368**, 387-403 (2006).
2. H. Braak, E. Braak, Neuropathological staging of Alzheimer-related changes. *Acta neuropathologica* **82**, 239-259 (1991).
3. D. R. Thal, U. Rub, M. Orantes, H. Braak, Phases of A -deposition in the human brain and its relevance for the development of AD. *Neurology* **58**, 1791-1800 (2002).
4. W. E. Klunk *et al.*, Imaging brain amyloid in Alzheimer's disease with Pittsburgh Compound-B. *Annals of neurology* **55**, 306-319 (2004).
5. M. A. Mintun *et al.*, [11C]PIB in a nondemented population: potential antecedent marker of Alzheimer disease. *Neurology* **67**, 446-452 (2006).
6. V. L. Villemagne, M. T. Fodero-Tavoletti, C. L. Masters, C. C. Rowe, Tau imaging: early progress and future directions. *Lancet neurology* **14**, 114-124 (2015).
7. J. A. Hardy, G. A. Higgins, Alzheimer's disease: the amyloid cascade hypothesis. *Science* **256**, 184-185 (1992).
8. C. R. Jack *et al.*, Tracking pathophysiological processes in Alzheimer's disease: an updated hypothetical model of dynamic biomarkers. *The Lancet Neurology* **12**, 207-216 (2013).
9. R. J. Bateman *et al.*, Clinical and biomarker changes in dominantly inherited Alzheimer's disease. *N Engl J Med* **367**, 795-804 (2012).
10. R. J. Perrin, A. M. Fagan, D. M. Holtzman, Multimodal techniques for diagnosis and prognosis of Alzheimer's disease. *Nature* **461**, 916-922 (2009).
11. E. S. Musiek, D. M. Holtzman, Three dimensions of the amyloid hypothesis: time, space and 'wingmen'. *Nature neuroscience* **18**, 800-806 (2015).
12. P. Giannakopoulos *et al.*, Tangle and neuron numbers, but not amyloid load, predict cognitive status in Alzheimer's disease. *Neurology* **60**, 1495-1500 (2003).
13. T. Gomez-Isla *et al.*, Profound loss of layer II entorhinal cortex neurons occurs in very mild Alzheimer's disease. *The Journal of neuroscience : the official journal of the Society for Neuroscience* **16**, 4491-4500 (1996).
14. M. Ingelsson *et al.*, Early A $\beta$  accumulation and progressive synaptic loss, gliosis, and tangle formation in AD brain. *Neurology* **62**, 925-931 (2004).
15. J. C. Morris, J. L. Price, Pathologic correlates of nondemented aging, mild cognitive impairment, and early-stage Alzheimer's disease. *Journal of molecular neuroscience : MN* **17**, 101-118 (2001).
16. M. Marquie *et al.*, Validating novel tau positron emission tomography tracer [F-18]-AV-1451 (T807) on postmortem brain tissue. *Annals of neurology*, (2015).
17. N. Villain *et al.*, Regional dynamics of amyloid-beta deposition in healthy elderly, mild cognitive impairment and Alzheimer's disease: a voxelwise PiB-PET longitudinal study. *Brain : a journal of neurology* **135**, 2126-2139 (2012).



18. H. Hampel *et al.*, Core candidate neurochemical and imaging biomarkers of Alzheimer's disease. *Alzheimer's & dementia : the journal of the Alzheimer's Association* **4**, 38-48 (2008).
19. J. C. Morris, The Clinical Dementia Rating (CDR): current version and scoring rules. *Neurology* **43**, 2412-2414 (1993).
20. D. T. Chien *et al.*, Early clinical PET imaging results with the novel PHF-tau radioligand [F-18]-T807. *Journal of Alzheimer's disease : JAD* **34**, 457-468 (2013).
21. Y. Su *et al.*, Quantitative analysis of PiB-PET with FreeSurfer ROIs. *PloS one* **8**, e73377 (2013).
22. Y. Su *et al.*, Partial volume correction in quantitative amyloid imaging. *NeuroImage* **107**, 55-64 (2015).
23. R. A. Sperling *et al.*, Toward defining the preclinical stages of Alzheimer's disease: recommendations from the National Institute on Aging-Alzheimer's Association workgroups on diagnostic guidelines for Alzheimer's disease. *Alzheimer's & dementia : the journal of the Alzheimer's Association* **7**, 280-292 (2011).
24. C. R. Jack, Jr. *et al.*, An operational approach to National Institute on Aging-Alzheimer's Association criteria for preclinical Alzheimer disease. *Annals of neurology* **71**, 765-775 (2012).
25. R. Lockhart, J. Taylor, R. J. Tibshirani, R. Tibshirani, A Significance Test for the Lasso. *Ann Stat* **42**, 413-468 (2014).
26. R. Tibshirani, Regression shrinkage and selection via the Lasso. *J Roy Stat Soc B Met* **58**, 267-288 (1996).
27. H. Zou, T. Hastie, Regularization and variable selection via the elastic net. *J Roy Stat Soc B* **67**, 301-320 (2005).
28. G. W. Small *et al.*, PET of brain amyloid and tau in mild cognitive impairment. *N Engl J Med* **355**, 2652-2663 (2006).
29. J. Shin, S. Y. Lee, S. H. Kim, Y. B. Kim, S. J. Cho, Multitracer PET imaging of amyloid plaques and neurofibrillary tangles in Alzheimer's disease. *NeuroImage* **43**, 236-244 (2008).
30. C. F. Xia *et al.*, [(18)F]T807, a novel tau positron emission tomography imaging agent for Alzheimer's disease. *Alzheimer's & dementia : the journal of the Alzheimer's Association* **9**, 666-676 (2013).
31. M. T. Fodero-Tavoletti *et al.*, 18F-THK523: a novel in vivo tau imaging ligand for Alzheimer's disease. *Brain : a journal of neurology* **134**, 1089-1100 (2011).
32. D. T. Chien *et al.*, Early clinical PET imaging results with the novel PHF-tau radioligand [F18]-T808. *Journal of Alzheimer's disease : JAD* **38**, 171-184 (2014).
33. M. Maruyama *et al.*, Imaging of tau pathology in a tauopathy mouse model and in Alzheimer patients compared to normal controls. *Neuron* **79**, 1094-1108 (2013).
34. N. Okamura *et al.*, Non-invasive assessment of Alzheimer's disease neurofibrillary pathology using 18F-THK5105 PET. *Brain : a journal of neurology* **137**, 1762-1771 (2014).

35. V. L. Villemagne *et al.*, In vivo evaluation of a novel tau imaging tracer for Alzheimer's disease. *European journal of nuclear medicine and molecular imaging* **41**, 816-826 (2014).
36. K. J. Friston, C. D. Frith, P. F. Liddle, R. S. Frackowiak, Functional connectivity: the principal-component analysis of large (PET) data sets. *Journal of cerebral blood flow and metabolism : official journal of the International Society of Cerebral Blood Flow and Metabolism* **13**, 5-14 (1993).
37. J. Hardy, K. Duff, K. G. Hardy, J. Perez-Tur, M. Hutton, Genetic dissection of Alzheimer's disease and related dementias: amyloid and its relationship to tau. *Nature neuroscience* **1**, 355-358 (1998).
38. L. K. Clinton, M. Blurton-Jones, K. Myczek, J. Q. Trojanowski, F. M. LaFerla, Synergistic Interactions between Abeta, tau, and alpha-synuclein: acceleration of neuropathology and cognitive decline. *The Journal of neuroscience : the official journal of the Society for Neuroscience* **30**, 7281-7289 (2010).
39. A. M. Fagan, D. M. Holtzman, Cerebrospinal fluid biomarkers of Alzheimer's disease. *Biomarkers in medicine* **4**, 51-63 (2010).
40. L. F. Maia *et al.*, Changes in amyloid-beta and Tau in the cerebrospinal fluid of transgenic mice overexpressing amyloid precursor protein. *Science translational medicine* **5**, 194re192 (2013).
41. D. K. Johnson, M. Storandt, J. C. Morris, J. E. Galvin, Longitudinal study of the transition from healthy aging to Alzheimer disease. *Archives of neurology* **66**, 1254-1259 (2009).
42. E. Grober, H. Buschke, H. Crystal, S. Bang, R. Dresner, Screening for dementia by memory testing. *Neurology* **38**, 900-903 (1988).
43. E. H. Rubin *et al.*, A prospective study of cognitive function and onset of dementia in cognitively healthy elders. *Archives of neurology* **55**, 395-401 (1998).
44. D. Wechsler, *WMS-R : Wechsler Memory Scale--Revised : manual*. (Psychological Corp. : Harcourt Brace Jovanovich, San Antonio, 1987), pp. viii, 150 p.
45. J. E. Doppelt, W. L. Wallace, Standardization of the Wechsler adult intelligence scale for older persons. *J Abnorm Psychol* **51**, 312-330 (1955).
46. H. Goodglass, E. Kaplan, *The assessment of aphasia and related disorders*. (Lea & Febiger, Philadelphia, ed. 2nd, 1983), pp. vii, 102, 131 p.
47. S. G. Armitage, *An analysis of certain psychological tests used for the evaluation of brain injury*. Psychological monographs: general and applied, (American Psychological Association, Washington,, 1946), pp. iii, 48 p.
48. A. M. Fagan *et al.*, Inverse relation between in vivo amyloid imaging load and cerebrospinal fluid Abeta42 in humans. *Annals of neurology* **59**, 512-519 (2006).
49. R. Tarawneh *et al.*, Visinin-like protein-1: diagnostic and prognostic biomarker in Alzheimer disease. *Annals of neurology* **70**, 274-285 (2011).
50. G. G. Roussas, *A first course in mathematical statistics*. (Addison-Wesley Pub. Co., Reading, Mass., 1973), pp. xv, 506 p.

51. C. E. Weatherburn, *A first course in mathematical statistics*. (The university press, Cambridge Eng., 1946), pp. xv, 271, 271 p.

**Table 1. Study Cohort Demographics.**

	T807 + Florbetapir	T807 + Florbetapir + CSF	T807 + Florbetapir + NP
N	46	36	40
Age (standard deviation)	75.4 (6.6)	76.3 (6.6)	75.7 (6.5)
M/F	30 / 16	25 / 11	27 / 13
CDR 0/0.5/ $\geq 1$	36 / 7 / 3	31 / 2 / 3	34 / 4 / 2
APOE $\epsilon 4+$	20	16	18

Demographics for the main cohort and two subsets. CSF=cerebrospinal fluid assay, NP= Neuropsychological Testing. APOE= apolipoprotein  $\epsilon$

## Figures and Figure Captions

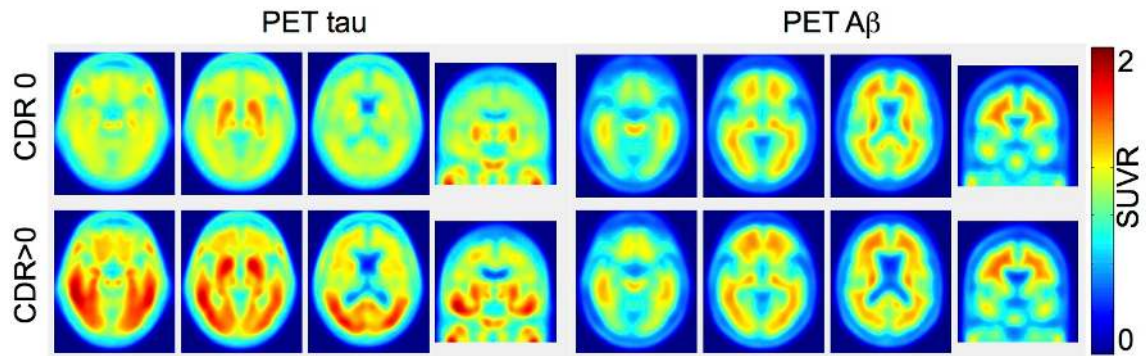


Figure 1. Mean positron emission tomography (PET) tau and A $\beta$  topographies in participants with and without clinical Alzheimer's disease (AD). Mean tau SUVR images averaged across participants with clinical dementia rating (CDR) 0 (top row) or CDR>0 (bottom row). Images are presented in radiological convention.

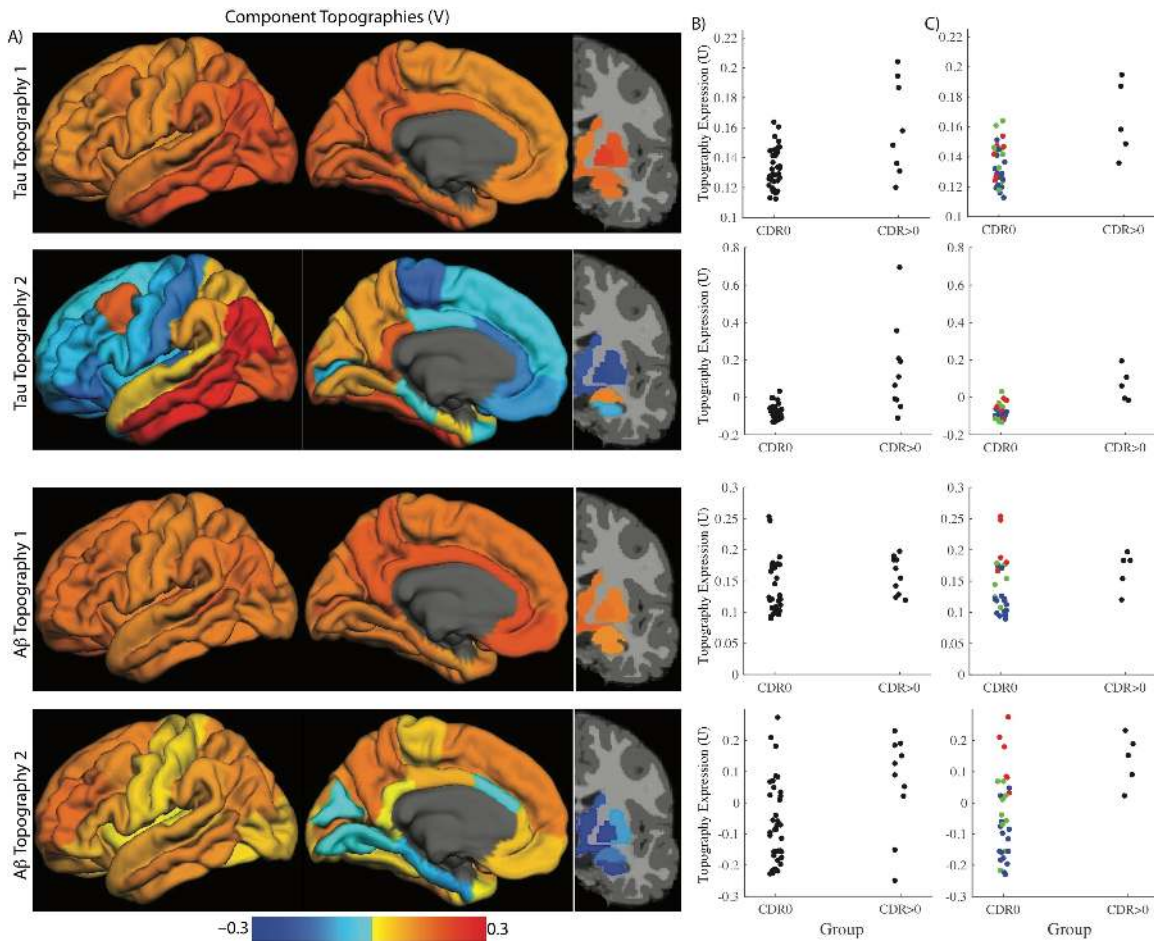


Figure 2. PET tau and A $\beta$  topographies are associated with disease severity. **A:** Right singular vectors ( $V$ ) of the singular value decomposition (SVD) of the regional PET tau and A $\beta$  data represented as topographies. The dimensionality of both tau and A $\beta$  was estimated to be two. The first topography for both PET species broadly represents the mean (i.e., all regions are homogeneously weighted). The second tau topography is present within the temporal lobe and the second A $\beta$  topography is largely seen in frontal and parietal lobes. Color bar represents regional weights within each singular component. **B:** The representations of these topographies in individuals (left singular vectors;  $U$ ), or put another way, the data original data projected onto these topographies, varies with CDR for both PET tau topographies

and the second PET A $\beta$  topography. Increasing disease severity (measured using the CDR) is associated with increasing representation of the present topographies in individuals. However, particularly in the A $\beta$  data, there is significant heterogeneity.

**C:** Similar graphs as (B) but only participants with CSF are included. Color in the CDR 0 group indicates preclinical disease status. Blue corresponds to healthy aging (i.e., no A $\beta$  or tau pathology), green corresponds to Stage 1, red corresponds to Stage 2.

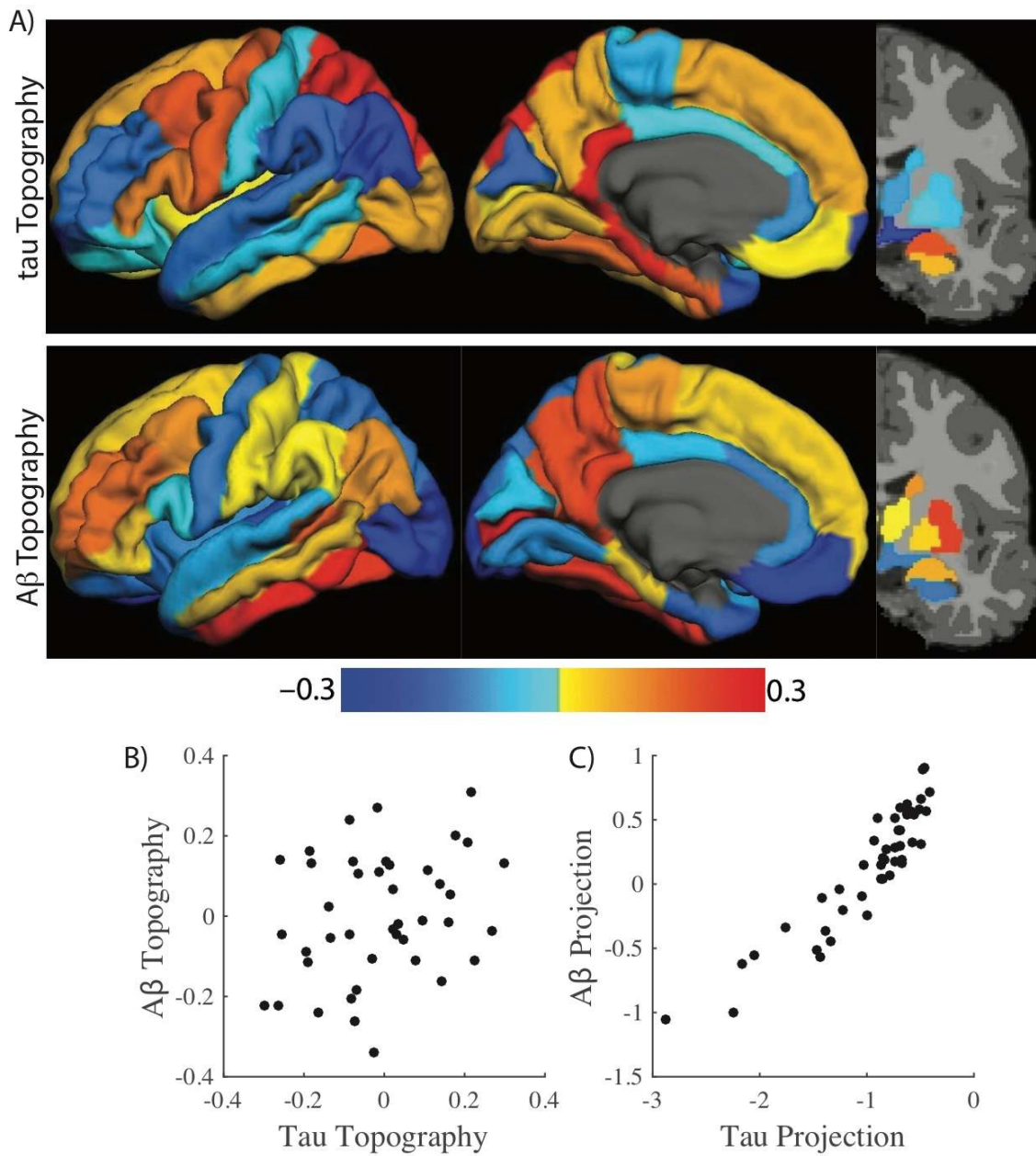


Figure 3. Tau and A $\beta$  in distinct topographies are strongly correlated. **A:** Topographies for PET tau and PET A $\beta$  derived from canonical correlations that maximize the correlation between PET tau and A $\beta$  deposition. **B:** Scatter plot of the weights on each region demonstrates that PET tau and A $\beta$  topographies are not



significantly related. This is consistent with the typical topographies of tau and A $\beta$  pathology being distinct. **C:** The data projected onto the canonical variables however reveals a robust positive relationship.

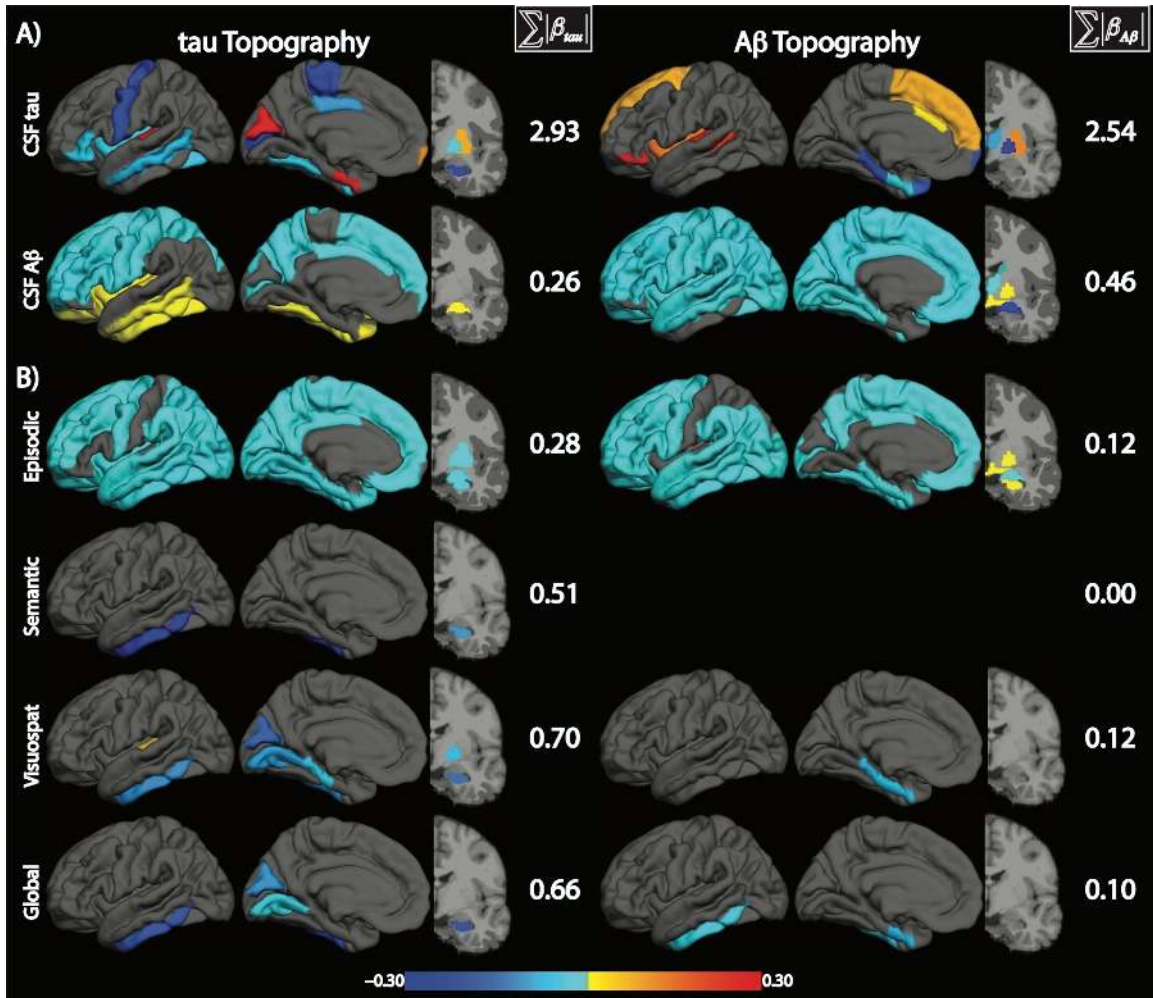


Figure 4: CSF and Neuropsychological Performance are predicted by tau and Aβ Topographies. Each row represents a single penalized regression model where either CSF protein levels or neuropsychological performance is predicted.  $\sum |\beta_{\tau}|$  and  $\sum |\beta_{A\beta}|$  represent the total predictive weight of tau and Aβ topographies, respectively. Grey regions have no predictive weight. A: Penalized regression models that predict CSF tau and Aβ<sub>42</sub> using tau and Aβ topographies. As CSF Aβ<sub>42</sub> levels are inversely related to amyloid burden, negative weights indicate regions where topographies predict worse CSF Aβ<sub>42</sub> pathology. B: Penalized regression

models that predict neuropsychological performance. Regions with negative values are where more PET pathology predicts lower cognitive performance.